Laser and Particle Beams (2009), *27*, 345–354. Printed in the USA.
Copyright © 2009 Cambridge University Press 0263-0346/09 $20.00
doi:10.1017/S0263034609000457

Theoretical calculation of atomic data for plasma spectroscopy

V. STANCALIE

National Institute for Laser, Plasma and Radiation Physics, Laser Department, Bucharest, Romania, Association EURATOM MEdC

(Received 24 January 2008; Accepted 3 March 2008)

Abstract

In the present article, a number of theoretical approximations and numerical methods, varying in complexity, are reviewed, in order to facilitate their selection for plasma diagnostic purposes. Results refer to highly charged ions, particularly in the lithium isoelectronic sequence. This article describes progress in understanding the role of laser induced degenerate state phenomenon on resonances obtained by using lasers. This type of process, implicitly included in the R-matrix Floquet calculation, contributes to some degree, to the overall behavior of the resonance profiles. The present article gives comparative results obtained from *ab initio* non-perturbative treatment and perturbative calculation of autoionization widths in Be-like ions. The effective oscillator strength for complex highly ionized atoms is, also, provided. Such calculations are of interest as they represent accurate benchmark data for beam emission spectroscopy, Zeff analysis, or complex atoms modeling in fusion plasma devices.

Keywords: Autoionization; Electron-ion collision; Laser-induced degenerate states

1. INTRODUCTION

Detailed knowledge of the structure of highly ionized atoms is essential for plasma spectroscopy. In the case of X-ray spectroscopy, most of atomic data currently used are produced using some of the simplest techniques. However, in a confrontation of plasma transport models with experiment and in spectral analysis, it is important to know the uncertainty in the collisional-radioactive coefficients. It is well-known, for example, that di-electronic recombination shifts equilibrium ionization balance fraction curves to higher temperature. This is most pronounced for the ions with one or two electrons outside the closed shells. It is also these ion fractions that show most markedly the effect of finite density reduction of the collisional radiative coefficients. This cannot be ignored for moderately ionized systems in plasmas with $N_e \geq 10^{10}$ cm^{-3}.

Highly ionized atoms have several properties that differ from those of neutral and few times ionized atoms. For example, there are large magnetic effects that cause the "fine structure" splitting to exceed the electrostatic structure separation. The allowed electric dipole transitions encounter strong competition from forbidden transitions. The transition rates for the forbidden decays scale with higher powers of Z than those of dipole transitions. The effects of quantum electrodynamics also scale with high powers of Z. Theoretical description of such effects involves the use of relativistic quantum mechanics and an accurate treatment of electron-electron correlation effects.

Collision between low energy electrons and atoms, molecules, or their ions are characterized by the formation of resonances and are often dominated by resonance mechanisms. Frequently, knowledge of the parameters defining the resonances participating in the process is sufficient to provide insight into details of the collisions. Referring to electron scattering Li-like ions, as an example, the contribution of di-electronic recombination process on gain of X-ray lasers with Li-like Al ions is mainly due to the capture of free electrons by ions in $1s^22s$ and $1s^22p$ configurations, producing autoionizing Be-like levels, which emit a photon to give bound levels of $1s^22snl$ and $1s^22pnl$ configurations. The most probably ways involve the autoionizing levels $1s^22pnl^{1,3}L'_J$ and $1s^23pnl^{1,3}L'_J$ (with initial ion $1s^22s$) and $1s^23dnl^{1,3}L'_J$ (with initial ion $1s^22p$) (Stancalie *et al.*, 1995). They can be characterized, respectively, by the core transitions $2s-2p$, $2s-3p$, and $2p-3d$. A major contribution to the cross-section involves the intermediate formation of doubly excited states of beryllium ions. The theoretical prediction of this process therefore depends on accurate information about the resonant states.

Address correspondence and reprint requests to: V. Stancalie, National Institute for Laser, Plasma and Radiation Physics, Laser Department, P. O. Box MG-36, Bucharest 077125, Romania. E-mail: viorica.stancalie@inflpr.ro

https://doi.org/10.1017/S0263034609000457 Published online by Cambridge University Press

This article pays particular attention to the calculation of atomic structure and scattering observable for Li-like ions, $1s^2nl$ configuration. A number of methods for atomic structure and electron-ion scattering calculations have been developed, which are able to provide atomic data for different spectroscopic applications. These methods vary in complexity and accuracy of the results in such way that one must decide between promptly available and highly accurate data to fulfill current spectroscopic needs.

In addition, this article shall address the role of laser induced degenerate state (LIDS) phenomenon on the behavior of resonance states of type $1s^22pns(^1P^0)$, $n = 9-12$, and respectively, $n = 5-12$ in Al X and C^{3+}. The work refers to particular situation when an electron colliding Li-like ion, is captured in the doubly excited state $1s^22pn's(^1P^0)$, belonging to Be-like ion. This state can decay by photon emission to an excited Rydberg state of type $1s^22sns$ (^1S) or can autoionize. These two states are studied throughout the resonant Rydberg series in a region where the autoionization and radiative rates are comparable in size. To this aim, it is analyzed the situation when these two excited Rydberg states are coupled by an intense, monochromatic, monomode, linearly polarized laser field.

This article is structured as follows. In Section 2, a short description of the well-known atomic structure calculation methods is given along with comparison between theoretical results and experimental data. In Section 3, the scattering calculation methods are reviewed. Electronic excitation and recombination cross-sections are needed for a variety of applications and their calculation places more emphasis on the accurate representation of target electron wave functions than the study of other processes. Calculations of the collision strengths are computationally demanding because of the dense Rydberg resonance structure below the highest target threshold. The low-temperature effective collision strength will be sensitive to the resonance structure. In this section are presented, comparatively, rate coefficients for electron impact excitation of Li-like Al ion as output from different theoretical approaches. In Section 4, special attention is paid to autoionization. Results are presented comparatively, from the *ab initio* non-perturbative and the perturbative treatment of this process. Conclusions will be outlined in Section 5.

2. ATOMIC STRUCTURE CALCULATION

The atomic structure problem is concerned with the computation of energy levels and rates of spontaneous transition among levels of the same ion (A—value) and from autoionizing levels of one ion to levels of the next ionized species (autoionization rates). There are several techniques used in atomic structure calculations: (1) model potential, (2) Hartree-Fock theory and method, (3) semiempirical methods, (4) perturbation methods, and (5) the R-matrix method in the close-coupling formalism.

Li-like ions are good systems for testing model potentials since, by having a single valence electron, their analysis leads to a single equation for the one-electron wave function. The solution of the Schrödinger equation based on this potential has been discussed by Bates and Damgaard (Sobelman *et al.*, 1981, and references herein). A generally applicable potential is the modified Thomas-Fermi potential. This potential is implemented in the computer program SUPERSTRUCTURE (Eisner *et al.*, 1974), which uses a scaled Thomas-Fermi-Dirac-Amadi potential. The scaling parameter is different for each angular momentum l. These parameters are iterated to give a minimum energy of a term or a group of terms. It should be noted that this method does not take into account correlation effects properly. Optimum Thomas-Fermi potential is obtained by minimizing the sum of the term energies. In contrast to the local central-field potentials, the Hartree-Fock methods (Pratt, 1956) entails the computation of the one-electron orbital in the non-local potential (direct and exchange) generated from electronic orbitals in a self-consistent manner using the variational principle. The accuracy of the wave function can be found by varying the valence orbitals while keeping the orbitals for the core fixed. This approximation has been developed to include electronic configurations interactions like in the multi-configuration Hartree-Fock (MCHF) (Froese Ficher, 1969) or in the superposition of configurations method (Hibbert, 1975).

The R-matrix method is the most accurate technique and takes into account additional effects that may contribute to atomic quantities, like configuration interactions and relativistic effects. The R-matrix formalism has been highly successful in describing a wide range of atomic and molecular scattering problems. The compilation volume by Burke and Berrington (1993), provide both a general review of the R-matrix method as applied to atomic and molecular collision processes and a very extensive bibliography. In the simplest version of this approach, the collision is considered separately according to whether the projectile is inside or external to the charge cloud of the target. The solutions obtained in each of these regions are related by the R-matrix that corresponds to the inverse of the logarithmic derivative of the wave function on the boundary of the two regions. This R-matrix is the basic solution of the electron scattering problem as it allows one to determine the atomic structure of the $(N + 1)$ system, the collision strengths, and photo-ionization cross sections. The total $(N + 1)$-electron wave function representing the electron-ion collision can be expanded in terms of R-matrix basis functions in the internal region in the form

$$\Psi_k = A \sum_{ij} \overline{\Phi_i} u_j a_{ijk} + \sum_j \chi_j b_{jk}. \quad (1)$$

Here $\overline{\Phi_i}$ is the channel functions formed by coupling the spin and the angular momenta of the scattered electron to the multi-configuration target wave functions, which form

https://doi.org/10.1017/S0263034609000457 Published online by Cambridge University Press

eigenstates of the total angular momentum L and total spin S. u_j is the continuum basis functions that are non-zero on the boundary of the internal region. χ_j is the $(N+1)$-electron quadratically integrable functions constructed from the same bound orbitals as target wave function. Finally, a_{ijk} and b_{jk} are the coefficients that are determined by diagonalizing the total Hamiltonian of the $(N+1)$-electron system in the basis defined by Eq. (1). The target wave functions and the $(N+1)$-electron quadratically integrable functions employed in Eq. (1) are constructed with a common set of one-electron spin-orbital functions. The radial part of each orbital is a sum of the Slater-type functions:

$$P_{nl}(r) = \sum_j C_{jnl} r^{I_{jnl}} \exp(-\xi_{jnl} r). \tag{2}$$

The internal region solution is obtained using the R-matrix II program package. In the external region, the asymptotic program STGF is used for the solution of the set of coupled differential equations.

In our previously works (Stancalie *et al.*, 1999, 2007; Stancalie, 2000; Stancalie & Pais, 2006), the superposition of configurations method and the model potential, respectively, have been used for different applications.

In the present article, we have carried out atomic structure calculations on the use of the semi-empirical method and the Cowan's code. Cowan (1981) summarized the progresses made in the analyses of atomic spectra with these methods. Semiempirical methods compute the atomic structure of ions solving simplified forms of the Hartree-Fock equations. One of the first examples of this approach is the Hartree-Fock-Slater scheme, which consists in replacing the two-electron non-local exchange terms of the Hamiltonian by the statistical potential function:

$$V_{xs}(r) = -\frac{3}{2}\left(\frac{24}{\pi}\rho\right)^{1/3}, \tag{3}$$

where ρ is the local electron density $\rho(r)$ of the atom. Cowan modified the Hartree-Fock-Slater approach to write the total potential of the ion as:

$$V^i(r) = -2Z/r + V_e(r) + V_{xs}(r), \tag{4}$$

where V_e is the potential energy for the density ρ-ρ_i of electrons, where i and V_{xs} are exchange terms in the form

$$V_{xs} = -k_1 f(r)\left[\frac{\rho'}{\rho' + k_2/(n-l)}\right]\left(\frac{\rho'}{\rho}\right)\left(\frac{24}{\pi}\rho\right)^{1/3}, \tag{5}$$

where k_1 and k_2 are constants, ρ' is the electron density less the densities of the electron i and of the electron with which it is paired, and

$$f(r) = \begin{cases} 1 & r \geq r_0 \\ 1 + k(1 - r/r_0) & r < r_0 \end{cases}, \tag{6}$$

for suitable k and r_0. This definition for the atomic potential is mostly empirically motivated and requires preconceived wave functions with which to construct the electron density functions ρ and ρ'. Once these functions are created and the atomic structure equations are solved in an iterative fashion. Then the accuracy of the results is assessed upon the agreement between obtained energy levels and oscillator strengths with a given sample of experimental values. The method has the advantage of being quite efficient, but it requires a lot of care in the construction of the initial electron density distribution. Further, it is difficult to estimate the accuracy of any given calculation except by the observed agreement of a limited sample of data with experimental values.

In Table 1 are presented comparatively, energy values (cm^{-1} units), calculated relative to the ground, for the lowest states belonging to Al^{10+}. These are to be compared with the available experimental data (Kelly, 1987).

3. SCATTERING CALCULATION

In considering the scattering calculation, it is customary to think of the residual ion as the "target" or "core" with N electrons and the incoming/outgoing (electron impact/photoionization) as "free" electron. Thus, the wave functions of the $(N+1)$-electron system can be expanded in terms of products of wave functions of the core and those of the electron. The resulting equations have to be solved for every value of the energy (k^2) and of the total angular momentum (L) of the $(N+1)$-electron system. This last condition motivates the so-called partial wave's expansion in which all states of

Table 1. *Calculated energies (in 10^3 cm^{-1} units) for the lowest states of type $1s^2nl_j(^2L_j)$ in Al^{10+} relative to the ground state. Results as output from the model potential, SCF, MCHF, and semi-empirical, methods are compared with experimental data (Exp.)*

k	$1s^2nl_j(^2L_j)$	E_k (10^3 cm^{-1}) Model potential	E_k (10^3 cm^{-1}) SCF method	E_k (10^3 cm^{-1}) MCHF method	E_k (10^3 cm^{-1}) Semi-empirical	E_k (10^3 cm^1) Exp.
1	$2s_{1/2}(^2S_{1/2})$	0.000	0.000	0.000	0.000	0.000
2	$2p_{1/2}(^2P_{1/2})$	180.155	175.201	175.259	176.378	176.01
3	$2p_{3/2}(^2P_{3/2})$	185.255	181.679	181.077	182.102	181.81
4	$3s_{1/2}(^2S_{1/2})$	2029.308	2013.283	2002.092	2024.803	2020.46
5	$3p_{1/2}(^2P_{1/2})$	2065.609	2061.340	2063.927	2073.290	2068.77

https://doi.org/10.1017/S0263034609000457 Published online by Cambridge University Press

definite angular momentum of the free electron are considered separately. Furthermore, the calculated collision strength is divided into partial waves as:

$$\Omega = \sum_{l=0}^{\infty} \Omega_l. \quad (7)$$

Collision strengths, phase shifts, and cross-sections may be obtained directly from the scattering K-matrices. We have applied this technique and an initial calculation using *LS* coupling with FARM (Burke & Noble, 1995)—a flexible asymptotic R-matrix package—has been performed (Stancalie & Pais, 2006), for solving the electron- scattering Li-like Al ion problem, in the external region of configuration space, where exchange effects may be neglected. The package uses a combination of R-matrix propagation techniques to ensure optimum stability and efficiency in integrating the coupled Schrödinger equations.

At lower impact energies, it is very difficult to compare the different theoretical results as the most sophisticated R-matrix results have large resonance structures below many of excitation thresholds. The effect of these resonances can be seen best by comparing excitation rates that are obtained by integrating the collision strength over a Maxwellian distribution of electron energies. The excitation rate coefficient for a transition from level i to level f at a temperature T_e is given by:

$$C(i \to f) = \frac{8.63 \cdot 10^{-6}}{g_i T_e^{1/2}} \int_{\Delta E}^{\infty} \Omega_E(i \to j) \exp(-E/kT_e) d(E/kT_e), \quad (8)$$

where $g_i = (2J_i + 1)$ is the statistical weight of the lower level i, $\Delta E = E_f - E_i$ is the excitation energy, $\Omega_E(I \to f)$ is the collision strength, k is the Boltzmann constant, and E is the electron impact energy. In Figure 1, are plotted the rate coefficients (in $\mathrm{cm^3\ s^{-1}}$) *versus* electron temperature (in eV), for electron impact excitation of $2s - 2p_{1/3}$ transition in Al^{10+}. The collision strengths have been calculated using the R-matrix code incorporated in atomic data and analysis structure (ADAS) package programs. Selected results for 100 eV are compared in Table 2 with those obtained from the Coulomb Born approximation (Sobelman, 1992). In this last case, the coupling between different target states is approximated by its asymptotic form at a large distance. This approximation is good for highly charged ions and transitions not affected by channel coupling and large partial waves.

Sobelman *et al.* (1981) suggested an approximate formula to obtain near threshold collision strengths for optically allowed transitions. The formula is based on the Kramers approximation and the Gaunt factor:

$$\Omega_{i,i'} = \frac{8\pi}{3\sqrt{3}} S_{ii'} \bar{g}, \quad (9)$$

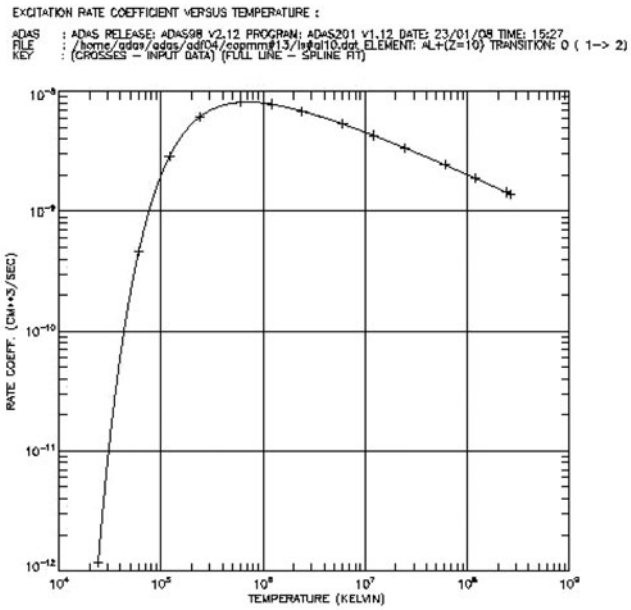


Fig. 1. Rate coefficient ($\mathrm{cm^3 s^{-1}}$) for electron impact excitation of $1s^2 2s - 1s^2 2p_{1/3}$ transition in Al^{10+} plotted versus electron temperature (in Kelvin units).

here $S_{i,i'}$ is the line strength, which relates to the absorption oscillator strength and $\bar{g}$ is the mean Gaunt factor. In the present article, we make use of perturbation theory and method (Poirier & Semoune, 1998), to evaluate the effective oscillator strength averaged over continuum and Gaunt factors, in the particular case of complex atoms with two electrons outside a closed shell. The method accounts for the general properties of the Coulomb Green's function together with its available compact integral representations, and discrete state expansions. The principle behind the theory is to use Sturmian representation of the Coulomb Green's function and the non-penetration hypothesis, assuming that, configuration mixing arising from perturbation by interaction is a small effect as long as the two wave functions are spatially separated. The advantage is that Sturmian term respects the same radial equation as bound-hydrogenic wave function.

Table 2. *The electron-impact excitation rate coefficient (in cm s^{-1} units) in Al^{10+}, at electron temperature of 100 eV. The upper levels energy relative to the ground is also indicated. The comparison refers to the Coulomb Born approximation and the R-matrix calculation results. (a^{-b} reads $a \times 10^{-b}$)*

Lower level	Upper Level	E (10^3 $\mathrm{cm^{-1}}$) Upper level (R-matrix)	C ($\mathrm{cm^3\ s^{-1}}$) Coulomb Born	C ($\mathrm{cm^3\ s^{-1}}$) R-matrix
$1s^2 2s$ ($^2S_{1/2}$)	$1s^2 2p(^2P_{1/2})$	176.72	2.92×10^{-09}	1.003×10^{-09}
	$1s^2 2p(^2P_{3/2})$	182.197	5.69×10^{-09}	5.211×10^{-09}
	$1s^2 3p(^2P_{1/2})$	2073.54	4.91×10^{-14}	7.503×10^{-12}
	$1s^2 3p(^2P_{3/2})$	2075.16	9.63×10^{-14}	1.494×10^{-11}
	$1s^2 4p(^2P_{1/2})$	2731.53	6.32×10^{-16}	9.030×10^{-13}

https://doi.org/10.1017/S0263034609000457 Published online by Cambridge University Press

The model refers to an atomic system, with the net charge of the core Z, and with two electrons outside the closed shell, the outer "Rydberg electron" labeled 1, being more excited than the inner electron, referred to as the "valence electron" and labeled 2. The other electrons, γ, are named core electrons. For example, Ba-like W^{18+} has configuration [Xe] $6s^2$, Sr-like W^{36+} has [Kr]$5s^2$, Hf-like W^{2+} has [Xe] $4f^{14}5d^26s^2$, etc. These configurations can be written as [Xe] $n_2l_2j_2n_1l_1$, for Ba-like and in a similar form for the others. The quasi-continuum spectra are simulated in "a single configuration description" assuming that, the Rydberg electron evolves from a bound hydrogenic state (n_1l_1) to a continuum state (εl) while, the valence electron falls from the excited ionic state $(n_2l_2j_2)$ to a lower state $(n_0l_0j_0)$.

The valence electron strongly interacts with the core. Hence the spin-orbit effect for this electron dominates all other interactions. The electronic repulsion $1/r_{12}$ is generally stronger than spin-orbit effects for the Rydberg electron. Based on the Heisenberg approximation for helium, the "bound" Rydberg state, $[\gamma]n_2l_2j_2n_1l_1$, has been written as zero-order solution for the eigenvalue equation, in the coordinate-space representation.

The "excited" Rydberg state of the atomic system, $[\gamma]n_0l_0j_0n_sl_s$, has been described in the Coulomb formalism accounting for the general properties of the Coulomb Green Function (CGF) and its Sturmian representation. In this case, the resolvent, $G(\Omega)$, of the non-relativistic Hamiltonian, $H_C = H_0 + V$, with $H_0 = p_0^2/2 + U(r_0) + p_s^2/2 - 1/r_s$, and $V = 1/r_{0s} - 1/r_s$, is a solution of the operator equation $(\Omega - H_C)\, G(\Omega) = 1$, where Ω is a complex energy variable, and G is the CGF. Then, the potential V can be treated as perturbation thus that, the dipole matrix elements between "bound" and "excited" Rydberg states, $[\gamma]n_2l_2j_2n_1l_1 \rightarrow [\gamma]n_0l_0j_0n_sl_s$, in intermediate coupling, can be written as the product of two mono-electronic matrix elements. Thus, the summation on the outer-electron principal quantum number can be performed exactly. The radial components of the Coulomb Sturmian functions are solutions of the equation:

$$\left[\frac{1}{r^2}\frac{d}{dr}r^2\frac{d}{dr} - \frac{l(l+1)}{r^2} - x^2\right]S_{n,l,x}(r) = -2nx\frac{1}{r}S_{n,l,x}(r), \qquad (10)$$

where the parameter x, $Re\, x > 0$, is kept fixed and n is a positive integer. Besides a normalization constant, the radial Sturmian functions have a structure similar to those of bound-state hydrogenic functions: $S_{n,l,x}(r) = N_{n,l}(x)\exp(-xr)(2xr)^l L^{2l+1}_{n-l-1}(2xr)$, where L^{2l+1}_{n-l-1} are Laguerre polynomials and the normalization factor reads: $N_{n,l}(x) = \frac{2x}{\sqrt{Z}}\sqrt{\frac{(n-l-1)!}{(n+1)!}}$. The expansion of G_l over the Sturmian basis reads explicitly: $G_l(r, r'; \Omega) = \sum_{n=l+1}^{+\infty}\frac{S_{n,l,x}(r)S_{n,l,x}(r')}{1-n/\tau}$. The dipole matrix elements $\langle S_{\nu_J, l_J}|r|S_{\nu_{J-1}, l_{J-1}}\rangle$, between Sturmian and/or hydrogenic radial components are always reducible to a combination of hypergeometric polynomials, which can be computed to within any chosen accuracy. Starting from the relation:

$$\langle n_1l_1|r^{-\kappa-1}|k_s;\, n_sl_s\rangle = \int_0^\infty dr r^{-\kappa+1}R(n_1l_1;\, r)S(k_s,\, n_sl_s;\, r), \qquad (11)$$

where

$$R(n_1l_1;\, r) = N(n_1l_1)r^{l_1}e^{-r/n_1}F(l_1+1-n_1;\, 2l_1+2;\, \frac{2r}{n_1}) \quad \text{and}$$

$$S(k_s,\, n_sl_s;\, r) = N(k_s,\, n_sl_s)r^{l_s}e^{-k_sr} \times F(l_s+1-n_s,\, 2l_s+2,\, 2\,k_sr)$$

$$N(n_1l_1) = \frac{2}{n_1^2}\frac{(2/n_1)^{l_1}}{(2l_1+1)!}\left(\frac{(n_1+l_1)!}{(n_1-l_1-1)!}\right)^{1/2} \quad \text{and}$$

$$N(k_s,\, n_sl_s) = \frac{(2\,k_s)^{l_s+1}}{(2l_s+1)!}\left(\frac{(n_s+l_s)!}{(n_s+l_s-1)!}\right)^{1/2}$$

The dipole matrix element is:

$$\begin{aligned}\langle n_1l_1|r^{-\kappa-1}|k_s,\, n_sl_s\rangle &= N(n_1l_1)N(k_s,\, n_sl_s)\\ &\times\frac{(2l_1+1)!}{(k_s+\frac{1}{n_1})^{l_1+l_s-\kappa+2}} \times \sum_{p=0}^{n_1-l_1-1}\binom{n_1-l_1-1}{p}\\ &\times\frac{(l_1+l_0-\kappa+p+1)!}{(2l_1+p+1)!}\times\left(\frac{-2/n_1}{k_s+1/n_1}\right)^p\\ &\times F\left(l_s+1-n_s,\, l_1+l_s-k+p+2,\, 2l_s+2;\, \frac{2\,k_s}{k_s+\frac{1}{n_1}}\right)\end{aligned} \qquad (12)$$

where $\binom{n}{m}$ is the binomial coefficient $= \frac{n!}{(n-m)!m!}$ and a_n is the Pochhammmer symbol $= 1$ *if* $n = 0$ and $a(a+1)\ldots(a+n-1)$ for positive integer n. If $m > n$ the second term is absent and the first sum ranges from $p = n$ to m.

The effective oscillator strength averaged over continuous spectrum can be defined as:

$$f_{eff} = \frac{f_{eff}(n_1)}{n_1},$$

where

$$\begin{aligned}f_{eff}(n_1) = \frac{2\,m}{3\hbar\, e^2}\cdot\frac{E_s}{2J+1}&\sum_{n_0,l_0,j_0,l_s}\sum_{n_s}\left|\langle n_2l_2j_2|r_2|n_0l_0j_0\rangle\right|^2\\ &\times\left|\left(\int_0^\infty dr R(n_1l_1;\, r)S(k_s,\, n_sl_s;\, r)\right)\right|^2.\end{aligned} \qquad (13)$$

In Eq. (13), the sum runs over the complete (discrete + continuous) set of eigenstates of H_C. The "averaged excitation energy," E_s, is given by: $E_s = E_{n_2l_2j_2} - E_{n_0l_0j_0} - 1/2n_1^2 = -k_s^2/2$, with $E_{n_2l_2j_2}$ and $E_{n_0l_0j_0}$ threshold energies. The $R(n_1l_1;\, r)$ and $S(k_s,\, n_sl_s;\, r)$ are hydrogenic and Sturmian radial components of the wave functions with

https://doi.org/10.1017/S0263034609000457 Published online by Cambridge University Press

respect to the valence ($n_1 l_1$) and continuum electron ($n_s l_s$), respectively, m and e are the electron mass and charge, respectively, and J is the total angular momentum of the initial state. Finally, the Gaunt, G, factors for ionization of level n_1 has been evaluated as: $G_i = 1 + f_{eff} \ln\left|1 + \frac{E4Ry}{\chi_1}\right|$, where E is the collision energy, χ_1 is the ionization energy of level 1, $\chi_1 = Ry/n_1^2$, and Ry = 13.6 eV.

In intermediate coupling, f_{eff} (n_1) depends on k but not on J, since the whole Hamiltonian is independent of the Rydberg-electron spin. The effective oscillator strengths averaged over continuum for Be-like Ar and Ba-like W, ions, in dipole approximation, are given in Table 3. The calculation refers to continuum states with n_s ranges from n_1 to 15. The accuracy of the numerical calculation depends on the accuracy of the parent ion energy calculation and on the performed infinite, but discrete, sum over n_s of term involving the overlap integral between hydrogenic and Sturmian functions. The last one has been controlled in a self-consistent manner on the basis of the partial sum rules of the averaged oscillator strengths. These rules are fulfilled only in the case when the photon frequency equals to the difference of the eigenvalue of the approximate Hamiltonian to the wave functions used in the calculation, (E_s), is substituted in the oscillator strengths, $f_{eff}(n_1)$. The parent energies have been evaluated combining quantum defect theory and R-matrix method (QDT/R-matrix) (Stancalie, 2005*a*) for C^{2+} and Al^{9+} ions, and from the Cowan's code for Ba-like W ion.

4. AUTOIONIZATION

4.1. *Ab Initio* Non-Perturbative Calculation of Laser-Induced Degeneracies Involving Autoionizing States in Li-Like Ions

Doubly excited states (resonances) offer a very suitable laser frequency regime within which to undertake investigative calculations that has already attracted interest. These resonance regions have been studied in the context of multiphoton transitions. There have been several theoretical methods introduced to describe multiphoton processes in atoms (Knight *et al.*, 1990; Cyr *et al.*, 1997; Kylstra *et al.*, 1998; Kylstra & Joichain, 1998; Fearnside, 1998; Paspalakis *et al.*, 2000). Of these calculations, only those employing the R-matrix Floquet (RME) method couple the field to the ion non-perturbatively, and only those of Latinne *et al.* (1995) and Cyr *et al.* (1997), explicitly investigated the laser-induced modification of doubly excited states, that is to say, the interplay of LIDS. Specifically, the frequency and the intensity of the light field can be adjusted such that the energy and the width of the dressed ground state coincide with the energy and width of a dressed autoionizing state.

Table 3. *The effective oscillator strengths, $f_{eff}(n_1)$, averaged over continuum for Be-like Ar and Ba-like W, ions, in dipole approximation. Continuum quantum number n_s range from n_1 to 15*

Ion	Transition	$f_{eff}(n_1)$	
W^{18+}	**[Xe]** $6p_{3/2}n_1h \rightarrow$ **[Xe]**$6s_{1/2}n_sg$	$k = 7/2$	$k = 9/2$
	$n_1 = 6$	1.028552	0.411421
	7	1.296603	0.518641
	8	0.292346	0.116938
Ar^{14+}	**[He]** $2p_{3/2}n_1d \rightarrow$ **[He]** $2s_{1/2}n_sp$	$k = 1/2$	$k = 3/2$
	$n_1 = 3$	0.126883	0.063441
	4	0.088255	0.044127

The LIDS phenomenon has been studied (Stancalie, 2005*a*, 2005*b*) for transitions of type $1s^2 2sns - 1s^2 2pn's$, $\Delta n = n - n' = 0$ (n, $n' = 9 - 12$) in Al X and $\Delta n = n - n' = 0$, 2 (n, $n' = 5 - 12$) in C^{3+}. The laser dresses the autoionizing state, the quasi-bound state, and the projectile electron. Following the RMF theory (Burke *et al.*, 1991) and code, at resonance, this dressing is dominated by the resonant coupling between these states so that the influence of the remaining states can be ignored. With this assumption, the problem is reduced to a model space consisting of a ground state of atom $|g\rangle$ (or some excited bound state of atom), an autoionizing state $|a\rangle$ and a continuum $|\in\rangle$. Results are analyzed with two state model of Latinne *et al.* (1995), which reproduces the behavior of the Floquet states, showing that the coupling *via* the continuum is more important than the direct dipole coupling between states. The laser is used to strongly couple the autoionizing state to excited Rydberg state and operates in restricted frequency, $\omega = \Delta E$ (core transition energy in the parent ion) intervals. In the limit of low field intensities, the width of the quasi-bound state is much smaller than the width of the autoionizing state and this particular value of the electron energy takes $E \cong E_g + \omega$, with E_g being the position of the ground state.

Floquet theory calculates quasi-stationary solution of time dependent Schrodinger equation for a monochromatic field equation. In the RMF approach, the time-dependent wave function is written in a Floquet-Fourier form, so that the time-dependent Schrödinger equation is transformed into a time-independent eigenvalue equation, in which atom-field coupling is treated in a fully non-perturbative manner. This implies that all the resonant couplings, as well as non-resonant and high-order laser-induced couplings, are fully accounted for. The principle behind the theory is to divide configuration space into two regions, an internal and an external region. The internal region is defined by a sphere of radius a, centered upon the nucleus of the ion, within which the full $(N + 1)$-electron problem is solved; that is, correlation and exchange effects are fully accounted for within this region of space where the charge distribution of the target ion is considered to be confined. The rest of configuration space is regarded as the external region. Here both exchange and correlation effects between the target atom and the outgoing photoelectron can be neglected. The latter electron now interacts with the residual atom through a long-range potential, expressed in a multipole expansion, in addition to the applied laser field. Since the RMF approach

https://doi.org/10.1017/S0263034609000457 Published online by Cambridge University Press

is a non-perturbative approach, the electric field, oscillating with laser frequency ω, is included *ab-initio* in the Hamiltonian. The time-dependent Schrödinger equation is solved by expanding the wave function as a Floquet-Fourier series. This yields a block structure of the Hamiltonian, each block corresponding to the absorption or emission of a specific number of photons. In the inner region, all angular symmetries with the correct parity and up to some suitably chosen maximum total angular momentum are present within each Floquet block. By diagonalizing the Hamiltonian matrix in the inner region in length gauge, the R-matrix at the boundary of the box (radius a) is obtained. This matrix transformed from the length to the velocity gauge, is propagated over the outer region to a radius a', where the long-range interactions are small. This transformation concerns only the outgoing photoelectron (the $(N+1)$th) since the residual target electrons are not present in this region of configuration space. At this radius, the R-matrix is matched with an asymptotic expansion of the wave function yielding the complex quasi-energy and autoionizing rates, E, and Γ, of the system as a complex quasi-energy $E_F = E - i\Gamma/2$.

The two-state model shows that the zero-field position of the autoionizing state changes with ω, being scaled at the complex energy $-\omega + E_a - i\Gamma_a/2$. The corresponding detuning is defined as $d = E_a - E_g - \omega$. For fixed values of the field intensity and frequency, the two quasi-energies become equal, giving rise to laser-induced degenerate states. In Figures 2–4 are shown, respectively, trajectories in the complex plane of the complex energies belonging to the $1s^22s9s(^1S) - 1s^22p9s(^1P^0)$ states in Al X, $1s^22s5s(^1S) - 1s^22p5s(^1P^0)$ states, and $1s^22s5s(^1S) - 1s^22p7s(^1P^0)$ states in C^{3+}, respectively. In these figures, b and r label the trajectories of the quasi-bound and resonant states of type $1s^22sns(^1S^e)$ and $1s^22pns(^1P^0)$. Detuning is indicated next to the curves in atomic units. For each frequency, there are two curves, one connected adiabatically with the quasi-bound state, the other with the autoionizing state. The corresponding curves have the same line type (solid or dashed) and are labeled by the frequency. Big circles denote the zero-field position of the autoionizing state. For transition with $n = 9$ (Fig. 2), the resulting complex energies are given for a few fixed values of the frequency, from 0.800 to 0.806 atomic units(au), and intensity up to 1×10^{14} W/cm^{-2}. The corresponding detuning is 0.8029 au. Figure 3 gives the motion of the complex energies in the complex plane for $1s^22s5s(^1S)$ and $1s^22p5s(^1P^0)$ states in C^{2+}. The intensity was varied from 0 to 1×10^{13} W/cm^{-2} (the intensity steps are of 5×10^{10} W/cm^{-2}). For C^{2+}, the inner region boundary radius was taken as $10a_0$. At this radius, using 30 continuum radial functions per channel moves the energy state $1s^22s5s(^1S^e)$ at -0.21394 au relative to $^2S^e$ ionization threshold. The real energy of the autoionizing state $1s^22p5s(^1P^0)$ is situated at 0.09496 au relative to $^2P^0$ ionization threshold. In Figure 4, the LIDS position is shown for transition with $\Delta n = 2$ in C^{2+}. The trajectories of the

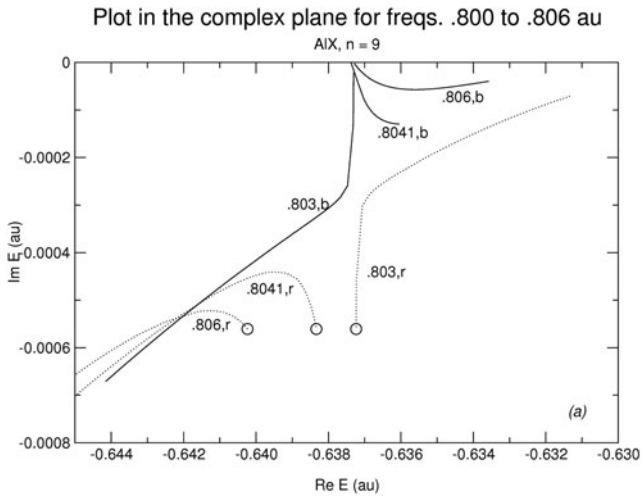


Fig. 2. The motion in the complex plane of the complex energies belonging to $1s^22s9s(^1S)$ (denoted by "b") and $1s^22p9s(^1P^0)$ (denoted by "r"), states in AlX as a function of frequency and field intensity. Corresponding curves have the same line type (solid or dashed) and are labeled by the frequency from 0.800 to 0.810 atomic units. Field intensity varied between 0.0 and 1×10^{14} W/cm^2 and is indicated next to the curves. Zero-field position of the autoionizing state is denoted by big circles. The energy scale is chosen such that $E_g = 0$.

complex energies of the $1s^22s5s(^1S)$ and $1s^22p7s(^1P^0)$ states are plotted in the complex plane, as a function of field intensity and frequency. For intermediate detuning, two structures are visible, about which the curves of the bound state and of the autoionizing state exchange their role. The atomic units are used and the energy scale is chosen such that ground-state energy is set to zero.

The results demonstrate that the motion of the trajectories in the complex plane shows different features of the coupled states. In all these figures, there is a critical point at the center of each of these two structures, at which the two complex

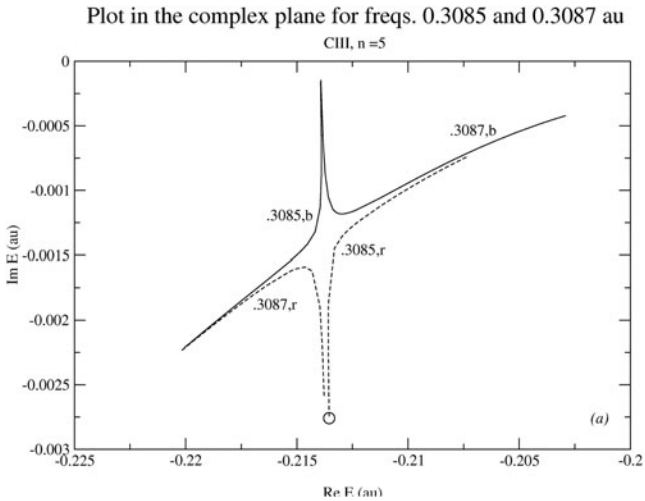


Fig. 3. Trajectories of the complex energies of $1s^22s5s(^1S^e)$, $1s^22p5s(^1P^0)$ states in C^{2+}, for frequencies 0.3085 and 0.3087 atomic units. The laser intensity is varied from 0.0 to 1×10^{13} W/cm^2.

https://doi.org/10.1017/S0263034609000457 Published online by Cambridge University Press

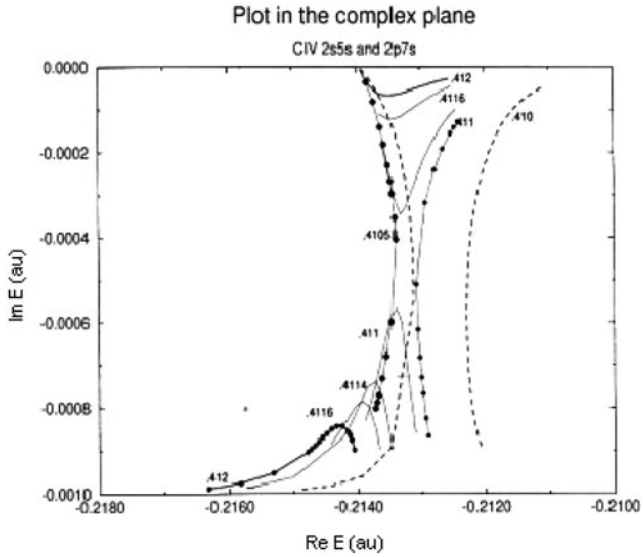


Fig. 4. Trajectories of the complex energies of $1s^2 2s5s(^1S^e)$ and $1s^2 2p7s(^1P^0)$ states as function of field intensity and frequency. For each frequency, there are two curves, one connected adiabatically to the "bound" and the other to the autoionizing state. The intensity is varied from 0.0 to 5×10^{13} Wcm^{-2}. The small dots give intensity in steps of 5×10^{11} Wcm^{-2}. At very small detunings (e.g., $\omega = 412$), the curve connected to the autoionizing state increases in width with intensity, while the bound state is "trapped" closed to the real axis. For intermediate detunings, two structures are visible, about which the curves of the 'bound' states and of the autoionizing state exchange their roles. The atomic units are used and the energy scale is chosen such that ground states energy is set to zero.

energies are exactly degenerate such that LIDS occurs. Closed to the LIDS position, the LIDS frequency for fixed intensity can be predicted as complex trajectories with a real part avoided crossing and an imaginary part crossing switch to having a real part crossing and an imaginary part avoided crossing as ω passes through the LIDS frequency. For frequencies near the LIDS frequency, the real part of the energy is nearly constant for low intensities up to the LIDS intensity, but the imaginary part changes rapidly converging together at the LIDS position. Beyond LIDS, the real and imaginary parts both diverge from each other. Considering our simple two-state model for C^{2+}, the values of E_g and E_a agree well with the opacity calculation. Table 4 gives comparison between the autoionization probability, Γ^a (meV), calculated for C^{3+}, with this simple model and those reported by more sophisticated numerical method (Berington *et al.*, 1998).

4.2. First-Order Perturbative Calculation in a Single-Configuration Approach

While an R-matrix-Floquet analysis was then successfully applied, one can discuss theoretical description of the process in a perturbative framework. The basic formalism using Coulomb Green's function in its analytical form has been described in Section 3. It can be applied with exact summation on the outer-electron principal quantum number. The

Table 4. *Comparison between calculated width, Γ^a, in meV units (meV), belonging to $1s^2 2pns(^1P^0)$ autoionizing states, $5 \leq n \leq 12$, in C^{3+}. Results refer to the R-matrix Floquet theory and code and its extension to LIDS method, and the R-matrix calculation by Berrington et al. (1998)*

n	Γ^a (meV) R-matrix-Floquet	Γ^a (meV) R-matrix
5	150	138
6	81	74
7	49	44
8	32	28
9	21.8	19
10	15.6	—
11	11.6	—
12	8.8	—

procedure has been suggested by Poirier (1994), Poirier and Semanoune (1998) and used for alkaline-earth-metal atoms. The principle behind the theory is to include second-order effects in autoionization-width computation using the Sturmian representation of the Coulomb Green's function after multipolar expansion of the interaction. The autoionization probability up to second order is given by the Fermi golden rule:

$$\Gamma = 2\pi \sum_{n_0 l_0 j_0 l} |A_1 + A_2|^2, \tag{14}$$

where (keeping notation given in Section 3) the first order amplitude reads:

$$A_1 = \sum_{t \geq l} \Omega(l_2, j_2, l_1; l_0, j_0, l; k; t) \times \langle n_2 l_2 j_2 | r^t | n_0 l_0 j_0 \rangle \langle n_1 l_1 | r^{-t-1} | \varepsilon l \rangle, \tag{15}$$

and

$$A_2 = \sum_{n_p l_p j_p l_s} \sum_{l_1 \geq l l_2 \geq 1} \langle n_2 l_2 j_2 | r^{t_1} | n_p l_p j_p \rangle \langle n_p l_p j_p | r^{t_2} | n_0 l_0 j_0 \rangle \times \Omega(l_2, j_2, l_1; l_p j_p, l_s; k; t_1) \times \Omega(l_p, j_p, l_s; l_0, j_0, l; k; t_2) \times \sum \int_\nu \langle n_1 l_1 | r^{-t_1 - 1} | \nu l_s \rangle \frac{1}{E_s - E(\nu)} \langle \nu l_s | r^{-t_2 - 1} | \varepsilon l \rangle \tag{16}$$

In Eq. (16), Ω is the angular factor in *jk* coupling, the infinite sum is over the quantum numbers of both electrons in a perturbing state $n_p l_p j_p \nu l_s$ and the sum over the principal quantum numbers of the perturbing states (n_p, ν) includes the discrete and continuous parts of the spectrum. In this equation $E_s = E_{n_2 l_2 j_2} - \frac{\zeta^2}{2n_1^2} - E_{n_p l_p j_p}$, where $E_{n_p l_p j_p}$ are the parent-ion energies, and ζ is the charge experienced by the outer electron whose energy is purely hydrogenic at zero order of the perturbation expansion.

https://doi.org/10.1017/S0263034609000457 Published online by Cambridge University Press

In atomic or molecular physics, it is customary the use of sum rules to handle the matrix elements that appear in many computations (Biedenharn & Rose, 1953; Biedenharn, 1955). These formulae are particularly well suited for the study of autoionization of large-angular momentum doubly excited Rydberg states. In Biedenharn's notation, the matrix element for bound-free transition is given by:

$$(\lambda, q; l) \equiv \int_0^\infty dr r^{-q} F_{\eta l} P_{nl+\lambda},$$

where $F_{\eta l}$ is a continuum wave function of energy $1/2\eta^2$ and angular momentum l and where $P_{nl+\lambda}$ is a discrete wave function of energy $-1/2n^2$ and angular momentum $l+\lambda$. The basic recursion relation for the radial matrix elements contains only radial integrals with $q-\lambda$ of a given parity. This relation allows the multipole $(\lambda-1, q+1; l+1)$ to be expressed using multipoles of the two preceding orders.

In order to compute the autoionization width for $1s^2 2pns(^1P^0)$, Rydberg states, $n = 9$–12 in Al^{10+} the starting point is the set of recursion relations on Coulomb non-relativistic wave functions:

$$\left[1+\left(\frac{l+1}{\eta}\right)^2\right]^{1/2} F_{\eta l} \equiv r^{-\alpha} \times \left(-1+\frac{(l+1)(l+1-\alpha)}{r}+(l+1)\frac{d}{dr}\right)\left(r^{\alpha} F_{\eta l+1}\right) \quad (17a)$$

$$-\left[1-\left(\frac{l+\lambda+1}{n}\right)^2\right]^{1/2} P_{nl+\lambda+1} = r^{-\beta}\left(1-\frac{(l+\lambda+1)(l+\lambda+1+\beta)}{r} + (l+\lambda+1)\frac{d}{dr}\right)\left(r^{\beta} P_{nl+\lambda}\right) \quad (17b)$$

with α, β arbitrary numbers chosen such that $q+\alpha+\beta=0$. Introducing these recursion relation in the matrix element difference will lead to a term proportional to the electric multipole $(\lambda-1, q+1; l+1)$ and terms involving derivatives that are recast in symmetric and antisymmetric expressions. The basic relation has been obtained by Poirier (1990) and contains only radial integrals with $q-\lambda$ of a given parity:

$$\left[1+\left(\frac{l+1}{\eta}\right)^2\right]^{1/2}\left(\lambda,q;l\right)-\left[1-\left(\frac{l+\lambda+1}{n}\right)^2\right]^{1/2} \times(\lambda,q;l+1)) = \frac{2l+\lambda+2}{2(q-1)}(\lambda-q)(\lambda-q+1) \times(\lambda-1,q+1;l+1)+\frac{\lambda(\eta^{-2}+n^{-2})}{2(q-1)}(\lambda-1,q-1;l+1). \quad (18)$$

Once dipolar matrix elements have been analytically computed and once quadrupole elements have been computed from recursion property with l decreasing from $n-2$ to 2, matrix elements of higher order can be derived from simple recursion relations. In Table 5, are presented results for the autoionization width of $1s^2 2pns(^1P^0)$ states in Al X, $n = 9$–11, as output from the RMF code, Cowan's code and from perturbative calculation.

5. CONCLUSION

In this article, a number of methods for atomic structure and electron-ion scattering calculations have been reviewed. Additionally, we have carried out semi-empirical and perturbative calculation to output values for the Gaunt factor, effective oscillator strengths, and autoionization rates. The simplest techniques developed in this article, of recursion relations on irregular electric multipoles, to describe excited Rydberg states, and the Coulomb Born approximation for electron –impact excitation rates, are particularly well suited for plasma when the evaluation of the ionic effective charge is requested. The single-electron description can be regarded in reasonable agreement with previously reported results. The approximation becomes more and more reliable as l increases and exchange effects are taken into account.

The article gives results from the non-perturbative treatment of laser induced degrade states. The motion of the complex energies in the complex plane as a function of the field intensity for different frequencies and atomic parameters gives complementary information on the role of LIDS on resonances obtained by laser. It is shown that the rate of ionization of the "ground" excited Rydberg state will first increase with intensity and then exhibit a typical "stabilization," namely a decrease of the ionization rate with increasing intensity. The most interesting is the critical region where a crossing (or an avoiding crossing) of trajectories occurs. The consequences of the one-photon LIDS as "trapping" of population at some non-zero field intensity and possible population transfer from the excited to autoionizing state in Li-like ions are under investigation. The effect of one-photon transition, that couples the autoionizing state to the degenerate continuum state *via* the stimulated emission and subsequent absorption of a photon, on the

Table 5. *Comparative results for the autoionization widths (in atomic units) of Rydberg states of type $1s^2 2pns(^1P^0)$, $n = 9$–11, in Al^{10+}. (a^{-b} reads $a \times 10^{-b}$)*

n	R-matrix Floquet method and its extension to LIDS	Recursion relations on irregular multipoles method This work	Superposition of configuration method (Cowan's code) This work
9	1.12132^{-03}	1.133604^{-03}	1.249251^{-03}
10	0.80882^{-03}	0.856664^{-03}	0.889504^{-03}
11	0.59559^{-03}	0.667035^{-03}	0.647273^{-03}

https://doi.org/10.1017/S0263034609000457 Published online by Cambridge University Press

resonance profile is studied as a function of the laser field intensity for particular case of Be-like Al and C ions. This type of process, implicitly included in the R-matrix Floquet calculation, contributes, to some degree, to the overall behavior of the resonance profiles. In the present case, the laser induced degenerate state phenomenon plays the most dominant role and is under consideration.

ACKNOWLEDGEMENTS

This work has been performed under the COST-ULTRA "Laser-matter interactions with ultrashort pulses, high-frequency pulses and ultra intense pulses. From attophysiscs to petawatt physics." Financial support under the Research Project "Pathways to Energy from Inertial Fusion – An Integrated Approach" is gratefully acknowledged.

The author gratefully acknowledges the support of The National University Research Council in carrying out part of this project.

REFERENCES

Berrington, K., Pelan, J. & Quigley, L. (1998). R-matrix calculation of CIII bound and continuum fine-structure states. *Phys. Scripta* **57**, 549–555.

Biedenharn, L.C. (1955). Quantum calculation of Coulomb excitation. I. *Phys. Rev*. **100**, 376–393.

Biedenharn, L.C. & Rose, M.E. (1953). Theory of angular correlation of nuclear radiations. *Rev. Mod. Phys*. **25**, 729–776.

Burke, P.G. & Berrington, K.A. (1993). *Atomic and Molecular Processes: An R-matrix Approach*. Bristol: IOP Publishing.

Burke, P.G., Francken, P. & Joichain, C.J. (1991). R-matrix Floquet theory of multiphoton processes. *J. Phys. B* **24**, 761–790.

Burke, V.M. & Noble, C.J. (1995). FARM- A flexible asymptotic R-matrix package. *Comput. Phys. Commun*. **85**, 471–500.

Cowan, R.D. (1981). *The Theory of Atomic Structure and Spectra*. (Sharp D.H. and Simmons L.M. Jr., eds.) Berkeley: University of California Press.

Cyr, A., Latinne, O. & Burke, P.G. (1997). R-MATRIX Floquet theory of multiphoton processes: IX. Three-photon laser-induced degenerate states in argon. *J. Phys. B*. **30**, 659–666.

Eissner, W., Jones, M. & Nussbaumer, H. (1974). Techniques for the calculation of atomic structure and radiative data including relativistic corrections. *Comput. Phys. Commun*. **8**, 270–306.

Fearnside, A.S. (1998). Intensity dependence of resonances profiles in multiphoton partial detachment rates of H^-. *J. Phys. B*. **31**, 275–288.

Froese Fischer, C. (1969). A multi-configuration Hartree-Fock program. *Comput. Phys. Commun.* **1**, 151–166.

Hibbert, A. (1975). CIV3–A general program to calculate configuration interaction wave functions and electric-dipole oscillator strengths. *Comput. Phys. Commun*. **9**, 141–172.

Kelly, R.L. (1987). Atomic and ionic spectrum lines of hydrogen through krypton. *J. Phys. Ref. Chem. Data*, **16**, 245–248.

Knight, P.L., Lauder, M.A. & Dalton, B.J. (1990). Laser-induced continuum structure. *Phys. Rept*. **190**, 1–61.

Kylstra, N.J. & Joichain, C.J. (1998). Double poles of the S matrix in laser-assisted electron-atom scattering. *Phys. Rev. A*. **57**, 412–431.

Kylstra, N.J., Paspalakis, E. & Knight, P.G. (1998). Laser-induced continuum structure in helium: *ab initio* nonperturbative calculations. *J. Phys. B*. **31**, L719–L728.

Latinne, O., Klistra, N.J., Dörr, M., Purvis, J., Terao-Dunsheath, M., Joichain, C.J., Burke, P.G. & Noble, C.J. (1995). Laser-induced degeneracies involving autoionizing states in complex atoms. *Phys. Rev. Lett*. **74**, 46–49.

Paspalakalis, E., Kylstra, N.J. & Knight, P.L. (2000). *Ab initio*, nonperturbative calculations of laser-induced continuum structure in helium. *Laser Part. Beams* **18**, 461–466.

Poirier, M. (1990). Recursion relations on irregular electric multipoles. *J. Phys. B.* **23**, 4071–4089.

Poirier, M. (1994). Exchange and fine-structure effects in autoionization of large-angular-momentum doubly excited Rydberg states. *Phys. Rev. A*. **50**, 1335–1347.

Poirier, M. & Semoune, R. (1998). Analysis of electronic correlations in large angular-momentum states using the Coulomb Green's function: excited states in alkaline-earth atoms. *J. Phys. B.* **31**, 1443–1461.

Pratt, G.W. (1956). Unrestricted Hartree-Fock method. *Phys. Rev*. **102**, 1303–1307.

Sobelman, I. (1992). *Atomic Spectra and Radiative Transitions* (Toennies, J.P., ed.). New York: Springer-Verlag.

Sobelman, I.I., Vainshtein, L.A. & Yukov, E.A. (1981). *Excitation of Atoms and Broadening of Spectral Lines* (Toennies J.P., ed.). New York: Springer-Verlag.

Stancalie, V. & Pais, V. (2006). Effective collision strengths for electron-impact excitation of Al^{10+}. *Laser Part. Beams* **24**, 235–240.

Stancalie, V. (2000). Fine-structure atomic data calculation for Al XI. *Phys. Sripta* **61**, 459–463.

Stancalie, V. (2005*a*). $1s^2 2ps$ ($^1P^0$) autoionizing levels in Be-like Al and C ions. *Phys. Plasmas* **12**, 043301.

Stancalie, V. (2005*b*). Complements to nonperturbative treatment of radiative damping effect in dielectronic recombination: $\Delta n = 2$ transition in CIV. *Phys. Plasmas* **12**, 10075.

Stancalie, V., Burke, V.M. & Sureau, A. (1999). Forbidden transitions in excitation by electron impact in Al Li-like ion. *Phys. Scripta* **59**, 52–54.

Stancalie, V., Pais, V., Totolici, M. & Mihailescu, A. (2007). Forbidden transitions in excitation by proton impact in Li-like Al ions. *Laser Part. Beams* **25**, 277–282.

Stancalie, V., Sureau, A., Klisnick, A., Moller, C., Guennou, H. & Berete, Y. (1995). Influence of dielectronic recombination on gain of X-ray lasers with Li-like ions. *Inst. Phys. Conf. Ser*. **140**, 129–132.

https://doi.org/10.1017/S0263034609000457 Published online by Cambridge University Press